



# Hydroaluminum Isocyanide Isomers: Prediction of Spectroscopic Properties

Pilar Redondo<sup>1</sup> , Miguel Sanz-Novo<sup>1,2</sup> , and Carmen Barrientos<sup>1</sup> <sup>1</sup> Computational Chemistry Group, Departamento de Química Física y Química Inorgánica, Facultad de Ciencias, Universidad de Valladolid, E-47011 Valladolid, Spain; [pilar.redondo@uva.es](mailto:pilar.redondo@uva.es)<sup>2</sup> Grupo de Espectroscopía Molecular (GEM), Área de Química-Física, Laboratorios de Espectroscopía y Bioespectroscopía, Parque Científico UVa, Unidad Asociada CSIC, Universidad de Valladolid, E-47011 Valladolid, Spain

Received 2021 December 2; revised 2022 February 10; accepted 2022 February 11; published 2022 March 28

## Abstract

Metal cyanides and isocyanides play a relevant role in the metal chemistry of the carbon-rich circumstellar envelope IRC+10216. It is thought that hydrometal cyanides/isocyanides could also be present in these environments; in fact, HMgNC has been detected in the same source that MgCN, MgNC, and AlNC. The aim of this work is to provide information about hydroaluminum cyanide/isocyanide. For this goal, a comprehensive analysis of the doublet and quartet potential energy surfaces of the [Al, C, H, N] system has been carried out. Different quantum chemistry methodologies from density functional theory to ab initio have been employed. For the [Al, C, H, N] isomers, the stability against dissociation and their interconversion processes have been analyzed. Our results show that the most relevant isomers from an experimental point of view are HAICN and HAINC. HAINC has been found to be the most stable isomer followed by HAICN, which is located at  $1.59 \text{ kcal mol}^{-1}$  ( $0.0689 \text{ eV}$ ) at the composite level. The interconversion process between HAICN and HAINC presents an energy barrier of  $10.0 \text{ kcal mol}^{-1}$  ( $5032 \text{ K}$ ) that makes this process not viable in the interstellar medium. We provide a complete set of relevant spectroscopic parameters for rotational spectroscopy for both HAICN and HAINC isomers using state-of-the-art quantum chemical computations, mandatory to guide an eventual laboratory or interstellar detection. Moreover, both isomers present sizable  $\mu_a$  dipole moment components ( $3.7$  and  $3.3 \text{ D}$ , respectively), which are large enough to enable a characterization by means of rotational spectroscopy, further increasing their interest as interstellar candidates.

*Unified Astronomy Thesaurus concepts:* [Astrochemistry \(75\)](#); [Interstellar molecules \(849\)](#); [Molecular spectroscopy \(2095\)](#)

## 1. Introduction

Heavy elements such as Na, K, Ca, Al, Fe or Ti, commonly denoted as “metals”, are important constituents of the interstellar medium (ISM), with Ca and Fe being the most heavily depleted elements in dense clouds and thus form a major component of interstellar dust (Mauron & Huggins 2010). The authors claim that the abundances of the uncondensed metal atoms that we observe are typically larger than the abundances of the metal-bearing molecules detected in the envelope and metal-bearing molecules play a key role in the metal chemistry.

The metal halides, NaCl, AlCl, KCl, and AlF were the first metal compounds identified in the circumstellar envelope of the carbon-rich mass-losing star IRC+10216 (Cernicharo & Juilín 1987). These molecules were previously predicted to be produced under local thermodynamical chemical equilibrium near the photosphere of carbon-rich evolved stars (Tsuji 1973). Guélin et al. (1986) discovered in the cool outer envelope of the carbon star IRC+10216 a new free radical, which was definitely identified as MgNC (Guélin et al. 1993; Kawaguchi et al. 1993). After that, other metal cyanides or isocyanides have been detected in the same source. Today the list of metal cyanides or isocyanides includes, NaCN (Turner 1991), MgCN (Ziurys et al. 1995), SiCN (Guélin et al. 2000), AlNC (Ziurys et al. 2002), SiNC (Guélin et al.

2004), KCN (Pulliam et al. 2010), FeCN (Zack et al. 2011), and CaNC (Cernicharo et al. 2019a). Related to these molecules the hydromagnesium isocyanide, HMgNC, and, recently, a pentatomic species, MgC<sub>3</sub>N, have been also detected (Cabezas et al. 2013; Cernicharo et al. 2019b).

The models dealing with the formation of metal-cyanide molecules in the outer shells of IRC+10216 consider a two-step mechanism starting with the radiative association of the metal ion ( $M^+$ ) with cyanopolyynes ( $NC_{2n+1}H$ ) and the subsequent dissociative recombination of the corresponding complex,  $M^+/NC_{2n+1}H$ , with electrons (Petrie 1996). The number of obtained metal-cyanide compounds depends on the branching ratios of the different fragmentation channels in the dissociative recombination that, in general, are not known. This model has been used to explain the abundances of the already detected species, MgNC, MgCN, HMgNC, and MgC<sub>3</sub>N (Cernicharo et al. 2019b).

In this context, aluminum is one of the most abundant elements (12th) in space. Its high degree of refractivity makes that in diffuse clouds an important amount is thought to be depleted into grains (Turner 1991; Mauron & Huggins 2010). Nevertheless, aluminum has an important gas-phase chemistry in carbon-rich circumstellar environments. As we have already indicated some aluminum-bearing molecules such as AlCl, AlF, (Cernicharo & Juilín 1987), and AlNC (Ziurys et al. 2002) have been detected. In addition, the radical AlO and the molecule AlOH have been also characterized toward the envelope of the oxygen-rich supergiant star VY Canis Majoris (VY CMa; Tenenbaum & Ziurys 2009, 2010).



Original content from this work may be used under the terms of the [Creative Commons Attribution 4.0 licence](#). Any further distribution of this work must maintain attribution to the author(s) and the title of the work, journal citation and DOI.

The presence in the cool outer envelope of the carbon star IRC+10216 of AINC and the fact that the identified species in this source, MgCN, MgNC, HMgNC, and MgC<sub>3</sub>N, have a common origin suggest that the HAlNC molecule should be a likely candidate for detection in space. There is scarce theoretical or laboratory data for hydrometal cyanide/isocyanide molecules that aid their characterization in space necessary to provide additional insights into the chemistry of metal-bearing isocyanides in space. From an experimental point of view, the rotational spectra of both isomers of the hydrides of silicon, HSiCN/HSiNC (Sanz et al. 2002), and the structure of hydride of zinc cyanide, HZnCN (Sun et al. 2009), were characterized in the laboratory. In addition, ab initio spectroscopic predictions were also reported for HZnCN/HZnNC (Redondo et al. 2015), HFeCN/HFeNC (Redondo et al. 2016), HTiCN/HTiNC (Redondo et al. 2019), and HCaCN/HCaNC (Redondo et al. 2020) systems.

In the last few years, high-level ab initio studies have been carried out on various aluminum-bearing molecules providing accurate theoretical electronic structures and spectroscopic parameters. Thus, a structural and spectroscopic investigation of tetratomic isomers comprising Al, N, C, and O atoms was carried out by Trabelsi et al. (2019). In their work, aluminum cyanate isomers were shown to be viable molecules for potential interstellar or circumstellar observation. The most stable isomer was determined to be linear aluminum isocyanate, AINCO, and a quasilinear cyanate isomer AIOCN was located 0.72 eV (at the CCSD(T)/CBS level) higher in energy with a notable kinetic stability, making it a viable candidate for astronomical observation. Similarly, Fortenberry et al. (2020) computed anharmonic vibrational frequencies and spectroscopic constants for OAIOH and AIOH molecules. Their work demonstrated the strong bonding yet floppy nature of Al–O bonds in the AIOH and OAIOH molecules and postulated OAIOH as a promising target for both millimeter and infrared observation. Recently, a high-level quantum chemical study of strongly bound inorganic species such as AlH<sub>2</sub>OH and AlH<sub>2</sub>NH<sub>2</sub> has been performed (Watrous et al. 2021), providing spectral data that could aid in the laboratory analysis and in the identification in space of these molecules.

On the other hand, astronomical discoveries have started a new era due to the development of modern astronomical facilities, i.e., the construction of new broadband receivers such as those of the Yebes-40 m radio telescope (18+ GHz bandwidth; Cernicharo et al. 2021a, 2021b), along with the implementation of new techniques, highlighting the line stacking and matched filtering approach (Lee et al. 2021; Loomis et al. 2021). Thus, in the last year, the number of detected interstellar molecules has grown almost exponentially (McGuire 2018 for a census). Within this framework, it is worth noticing that purely theoretical data have enabled to guide astronomical observations and detections of new interstellar species by using the spectral line survey as a “conventional” laboratory spectrum (Cernicharo et al. 2019b, 2021b; Pardo et al. 2021a). Moreover, new observations are steadily being carried out, highlighting the ultradeep spectral survey of IRC+10216 (Pardo et al. 2021b), which appear as very interesting data to look for the target species. Nevertheless, the identification of new molecules in the ISM usually relies on a preliminary spectroscopic characterization in the laboratory.

In this context, once we had deciphered the isomeric and conformational space of the [Al, H, C, N] system, we provided a high-level computed set of rotational spectroscopic parameters for the most stable HAICN and HAINC interstellar candidates to guide the spectral searches. In addition, to shed light into the stability of these molecules in space, we carried out a detailed analysis of the interconversion processes between isomers and dissociation energies.

## 2. Computational Methods

We began the study by performing a detailed search for the stable structures on the doublet and quadrupole potential energy surface (PES) of the [Al, H, C, N] system using the density functional theory (DFT). Specifically, the B3LYP (Becke 3 parameter Lee-Yang-Parr) functional (Becke 1988; Lee et al. 1988), and the double hybrid B2PLYP functional (Grimme 2006), which includes Hartree–Fock exchange and a perturbative second-order correlation part, have been employed. Geometric optimizations for the fundamental states of the isomers have also been performed using the double-hybrid functional B2PLYP combined with Grimme’s D3BJ dispersion B2PLYPD3 (Grimme et al. 2011) and the ab initio CCSD(T) (coupled cluster with single and double excitations including triple excitations through a perturbative treatment) level (Raghavachari et al. 1989).

The Pople’s triple-zeta 6-311++G(3df,2p) basis set (Hehre et al. 1986), which includes both polarization and diffuse functions on heavy atoms and hydrogen, was used in the B3LYP calculations. For the B2PLYP, B2PLYPD3, and CCSD(T) calculations, we employed the Dunning’s correlation consistent basis sets, aug-cc-pVTZ (Dunning 1989; Woon & Dunning 1993), which also includes both polarization and diffuse functions on all elements.

On each optimized structure at the abovementioned methods, harmonic vibrational frequencies were calculated to characterize the stationary points as minima (all real frequencies) or transition state structures (one frequency imaginary) and estimate the zero-point vibrational energy (ZPVE).

For the most relevant isomers from an experimental point of view, hydroaluminum cyanide/isocyanide, HAICN/HAINC, more precise structural parameters and energies were calculated. Geometry optimizations and vibrational frequencies were computed at the explicitly correlated coupled cluster theory with singles, doubles, and perturbative triplet CCSD(T)-F12 level (Knizia et al. 2009) in conjunction with the cc-pVTZ-F12 basis set (Peterson et al. 2008). This methodology is shown to correctly reproduce the molecular geometry of different metal bearing species (Cernicharo et al. 2019b). In addition, a composite approach like those used in previous works on metal cyanides and aluminum compounds (Redondo et al. 2016, 2019, 2020; Trabelsi et al. 2019; Fortenberry et al. 2020; Watrous et al. 2021) was applied. Composite approaches rely on the assumption that an estimated property can be obtained as a sum of additive contributions. We took as reference the CCSD(T) calculations with the aug-cc-pVTZ for C, N, and H or aug-cc-pV(Q+d)Z for Al (Dunning et al. 2001) basis sets. The estimated geometrical parameters or rotational equilibrium constants, denoted as  $P(\text{comp})$ , were obtained as:

$$P(\text{comp}) = P(\text{CBS}) + \Delta P(\text{CV}) + \Delta P(\text{DK}), \quad (1)$$

where  $P(\text{CBS})$  corresponds to the complete basis set (CBS) limit extrapolated value that considers basis-set truncation

errors. This is computed from the  $n^{-3}$  extrapolation equation (Helgaker et al. 1997) applied to the cases of  $n=4$  (Q) and  $n=5$  (5), using CCSD(T)/aug-cc-pV(Q+d)Z and CCSD(T)/aug-cc-pV(5+d)Z data, respectively.

The term,  $\Delta P(\text{CV})$ , accounts for core–valence (CV) effects. It is calculated taking the difference between a calculation including all electrons (ae) and a frozen-core (fc) approach:

$$\begin{aligned} \Delta P(\text{CV}) = & P(\text{ae} - \text{CCSD(T)/aug-cc-pCVQZ, all}) \\ & - P(\text{fc} - \text{CCSD(T)/aug-cc-pCVQZ}). \end{aligned} \quad (2)$$

The last term,  $\Delta P(\text{DK})$ , accounts for relativistic effects and is evaluated through Douglas–Kroll-type calculations (Douglas & Kroll 1974; Peng & Hirao 2009) at the CCSD(T) level in conjunction with the basis set cc-pVTZ-DK, as:

$$\begin{aligned} \Delta P(\text{DK}) = & P(\text{CCSD(T)} - \text{DK/cc-pVTZ} - \text{DK}) \\ & - P(\text{CCSD(T)/cc-pVTZ}). \end{aligned} \quad (3)$$

In addition, in the computation of composite energies we included the term corresponding to the ZPVE estimated at the CCSD(T)/aug-cc-pVTZ within the anharmonic approach:

$$E(\text{comp}) = E(\text{CBS}) + \Delta E(\text{CV}) + \Delta E(\text{DK}) + \text{ZPVE}. \quad (4)$$

To provide information with sufficient accuracy to be useful to spectroscopists in a possible laboratory identification by IR spectroscopy, anharmonic corrections were estimated for the two most stable isomers at the CCSD(T)/aug-cc-pVTZ level of theory using the second-order vibrational perturbation theory (VPT2; Mills 1972) within the context of the Watson Hamiltonian (Watson 1968). A full cubic force field (CFF) and semidiagonal quartic force constants have been included in the procedure. From the CFF calculations, we have computed vibration–rotation interaction constants.

The second-order Møller–Plesset (MP2) method (Møller & Plesset 1934) in conjunction with the aug-cc-pVQZ basis set was employed for calculating the electron-spin-rotation ( $\epsilon$ ) parameters and the nuclear-spin-rotation (C) constants.

Finally, to check the viability of our single reference calculations the T1 diagnostic at the CCSD(T) level was calculated (Lee & Taylor 1989). For the two most stable isomers, HAICN and HAINC, the obtained T1 diagnostic are 0.0167 and 0.0174, respectively. In addition, complete active space multiconfiguration self-consistent field (CASSCF; Werner & Knowles 1985a, 1985b) calculations have been performed and the weights of leading configuration of the complete active space wave function,  $c_0^2$ , are 0.910 and 0.912 for HAICN and HAINC, respectively. These values are greater than 0.90 (Jiang et al. 2012), and therefore both HAICN and HAICN molecules do not possess significant multireference character.

Quantum calculations were carried out using methods as implemented in the GAUSSIAN 16 program package (Frisch et al. 2016), MOLPRO (Werner et al. 2012, 2015), and the CFOUR Program (Stanton et al. 2013).

### 3. Results and Discussion

We will begin in Section 3.1 with an exhaustive analysis of the system [Al, H, C, N] on the doublet and quartet PESs to establish the ground state and relative energy of the located structures. Their interconversion and dissociation processes will be calculated in the Section 3.2. Finally, in Section 3.3, a

prediction of spectroscopic parameters for the most reliable isomers, from an experimental point of view, are reported.

#### 3.1. Structure and Energetics

We have located the stable structures on the doublet and quartet [Al, C, H, N] PESs using different methodologies. All the possible rearrangements, linear or bent structures with the aluminum atom located at one end of the chain or in a middle position, and cyclic (three-member ring) structures, with molecular formula [Al, C, H, N] are searched. Geometries are first optimized at the B3LYP/6-311++G(3df,2p) and B2PLYP/aug-cc-pVTZ levels and then for the ground state of each isomer additional optimizations at the B2PLYPD3/aug-cc-pVTZ and CCSD(T)/aug-cc-pVTZ are also performed. Harmonic vibrational frequencies are computed on the optimized geometries at each level. The CCSD(T)/aug-cc-pVTZ optimized geometries for the different [Al, C, H, N] isomers are shown in Figure 1. For each isomer, we have only included in Figure 1 the structures corresponding to their lowest-lying state (doublet or quartet).

We can see in Figure 1 the 11 minima characterized in their doublet or quartet PES. The first three isomers, HAICN, HAINC, and c-H-AINC, arise from the interaction between the aluminum atom of hydroaluminum, HAl, and the cyano radical. When the interaction takes place in the line of the C–N bond through either the carbon atom or the nitrogen atom hydroaluminum cyanide/isocyanide, HAICN/HAINC, bent structures are yield, whereas if the interaction is through the C–N bond, a three-member cyclic structure, c-H-AINC, is formed. The other two cyclic isomers, c-H-CAIN and c-H-NAIC, can be seen as the result of the interaction of the aluminum atom through the C–N bond of hydrogen cyanide/isocyanide, HCN/HNC. When the interaction of aluminum takes place with terminal atom N/C or hydrogen of HCN/HNC, leads to the linear or bent structures AINCH/AICNH or AIHCN/AIHNC, respectively. The last two structures, HCAIN and HNAIC, arising from the insertion of the aluminum atom into the carbon–nitrogen bond of HCN or HNC.

The relative energies (taking the most stable isomer as reference) computed at different levels of theory for the [Al, C, H, N] isomers are reported in Table 1. Regardless the computational level, we have obtained the same stability behavior, with hydroaluminum isocyanide in its doublet state, HAINC ( $^2A'$ ), as the lowest-lying isomer, followed by hydroaluminum cyanide, HAICN ( $^2A'$ ), which is only 1.18 kcal mol $^{-1}$  above, at the CCSD(T)/aug-cc-pVTZ level. A comparison of the relative energies computed at the different calculation levels with those calculated at the highest level, CCSD(T)/aug-cc-pVTZ, shows that the results obtained with the B2PLYP functional are closer to the CCSD(T) than those calculated with the B3LYP one. We observe that the inclusion of the Grimme’s D3BJ dispersion through the B2PLYPD3 level is not relevant for these systems, its inclusion causes changes in relative energies around 0.1 kcal mol $^{-1}$ . The largest deviations, as expected, are found for the isomers AIHCN and AIHNC (0.31 kcal mol $^{-1}$  and 0.53 kcal mol $^{-1}$ , respectively), which have a very large Al–H distance. We can also see that the relative energies obtained at the CCSD(T) level on the B3LYP optimized structures are very close to those calculated on the CCSD(T) ones. On the other hand, we obtain that doublet electronic states are more stable than the quartet ones, with the only exception of the less stable isomers HCAIN and

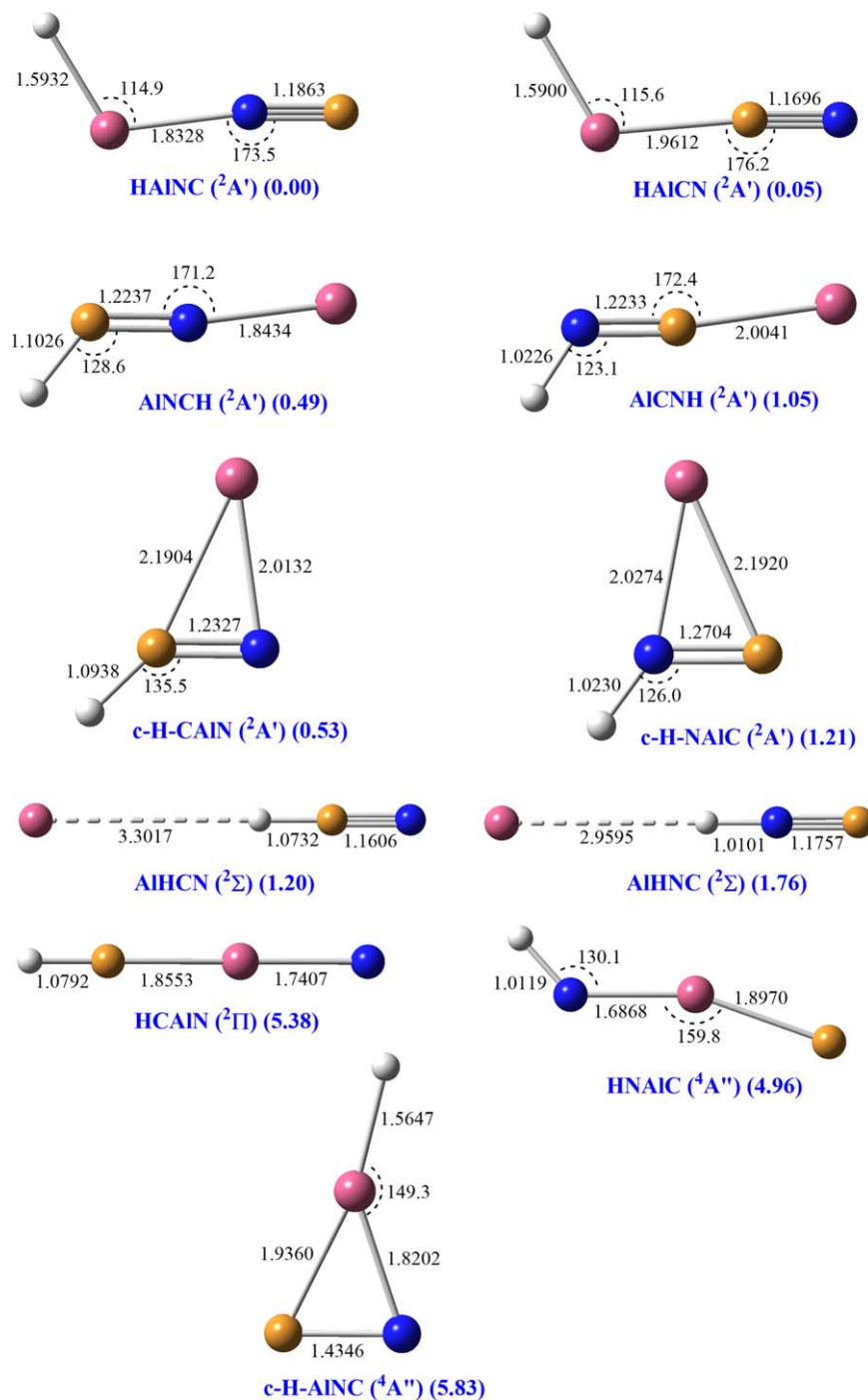


**Figure 1.** Optimized structures (distances in Angstroms and angles in degrees) at the CCSD(T)/aug-cc-pVTZ level for the [Al, C, H, N] isomers. Relative energies (in eV) are shown in parentheses. Optimized geometries and relative energies for HCAIN and HNAIC are calculated at the B2PLYP/aug-cc-pVTZ level.

HNAIC where the quartet state is slightly more stable than the doublet one. These isomers are located more than  $100 \text{ kcal mol}^{-1}$  above HAINC ( $^2A'$ ) isomer, and they are not relevant from an experimental point of view. It is worth noticing that, on the quartet PES the bent structure HAINC is not a true minimum, the optimization leads to the cyclic isomer c-H-AICN ( $^4A''$ ). This cyclic structure is not a minimum on the doublet PES.

The six isomers that arise from the interaction, either linear or through the C–N bond, between the aluminum atom and hydrogen cyanide/isocyanide HCN/HNC are located above

hydroaluminum cyanide/isocyanide, HAICN/HAINC. If we analyze the energies shown in Table 1, we can see that the isomers corresponding to the interaction of aluminum with HCN (AINCH, c-H-CAIN and AIHCN) are more stable than those that arise from the interaction with HNC (AICNH, c-H-NAIC, and AIHNC). The energy differences between analogous (cyanide/isocyanide) isomers range between  $12.85 \text{ kcal mol}^{-1}$  and  $15.73 \text{ kcal mol}^{-1}$  (e.g., AINCH is  $12.85 \text{ kcal mol}^{-1}$  more stable than AICNH, at the CCSD(T)/aug-cc-pVTZ level). The linear interaction of aluminum with N/C (to give AICNH or AINCH) is slightly more favorable

**Table 1**

Relative Energies (in kcal mol<sup>-1</sup>) for the [Al, C, H, N] Isomers at Different Levels of Theory. ZPV Energies are Included. The aug-cc-pVTZ Basis Set was Used Except for the B3LYP Calculation where the 6-311++G(3df,2p) one was Employed

Isomer	State	Level				
		B3LYP	CCSD(T) <sup>a</sup>	B2PLYP	B2PLYPD3	CCSD(T)
HAINC	<sup>2</sup> A'	0.00	0.00	0.00	0.00	0.00
	<sup>4</sup> A''	106.03	109.44	110.09		
HAICN	<sup>2</sup> A'	2.06	1.21	0.87	1.00	1.18
AINCH	<sup>2</sup> A'	7.67	11.28	9.60	9.56	11.37
	<sup>4</sup> A''	65.12	67.22	67.78		
AICNH	<sup>2</sup> A'	20.79	24.00	23.19	23.18	24.22
	<sup>4</sup> A''	63.46	64.32	65.22		
c-H-CAIN	<sup>2</sup> A'	11.48	12.19	12.01	12.12	12.28
	<sup>4</sup> A''	74.81	72.09	74.81		
c-H-NAIC	<sup>2</sup> A'	26.95	27.85	28.64	28.76	28.01
	<sup>4</sup> A''	87.76	86.98	89.36		
AIHCN	<sup>2</sup> Σ	29.71	27.79	28.62	29.31	27.62
	<sup>4</sup> Π	118.20	108.06	114.70		
AIHNC	<sup>2</sup> Σ	41.54	40.39	41.79	42.26	40.50
	<sup>4</sup> Π	130.81	121.45	128.71		
HCAIN	<sup>2</sup> Π	121.85	124.05			
	<sup>4</sup> Π	120.45	123.94			
HNAIC	<sup>2</sup> A'	122.25	125.95			
	<sup>4</sup> A''	117.16	114.45			
c-H-AICN	<sup>4</sup> A''	132.98	134.50	135.79	136.09	134.54

**Note.**

<sup>a</sup> Calculated on the optimized geometry at the B3LYP/6-311++(3df,2p) level.

**Table 2**

Structural Parameters (Distances in Angstroms and Angles in Degrees) and Relative Energies (in kcal mol<sup>-1</sup>) of the Lowest Lying [Al, C, H, N] Isomers at Different Levels of Theory

Level of calculation	CN	AIC	AIN	AIH	<AICN	<HAIC	<AINC	<HAIN	ΔE
HAINC									
CCSD(T)/cc-pVTZ	1.1865		1.8303	1.5931			174.0	114.9	0.00
CCSD(T)/aug-cc-pVTZ	1.1863		1.8328	1.5932			173.5	114.9	0.00
CCSD(T)/aug-cc-pVQZ	1.1831		1.8264	1.5892			173.8	114.7	0.00
CCSD(T)/aug-cc-pV(Q+d)Z	1.1831		1.8239	1.5876			173.5	114.7	0.00
CCSD(T)/aug-cc-pV(5+d)Z	1.1822		1.8225	1.5871			173.5	114.7	0.00
CCSD(T)F12a/cc-pVTZ-F12	1.1825		1.8216	1.5871			173.4	114.7	0.00
Composite	1.1785		1.8133	1.5807			173.6	114.5	0.00
HAICN									
CCSD(T)/cc-pVTZ	1.1696	1.9591		1.5900	176.6	115.6			1.09
CCSD(T)/aug-cc-pVTZ	1.1696	1.9612		1.5900	176.2	115.6			1.18
CCSD(T)/aug-cc-pVQZ	1.1663	1.9554		1.5860	176.2	115.4			1.47
CCSD(T)/aug-cc-pV(Q+d)Z	1.1666	1.9536		1.5841	176.1	115.4			1.49
CCSD(T)/aug-cc-pV(5+d)Z	1.1656	1.9520		1.5840	176.0	115.4			1.47
CCSD(T)F12a/cc-pVTZ-F12	1.1658	1.9512		1.5839	176.1	115.4			1.46
Composite	1.1620	1.9421		1.5777	175.9	115.2			1.40

than that occurring through the C–N bond; the energy difference between AINCH and c-H-CAIN is 0.91 kcal mol<sup>-1</sup>, and that of AICNH and c-H-NAIC is 3.73 kcal mol<sup>-1</sup> at the CCSD(T)/aug-cc-pVTZ level. Finally, the least stable isomers, AIHCN and AIHNC, are obtained from the linear interaction of Al with the H atom of HCN or HNC. The high values obtained for the Al–H distances (Figure 1) in the AIHNC and AIHCN isomers (3.3017 and 29595 Å, respectively) suggest that these compounds can be seen as intermolecular complexes between the Al atom and the HCN/HNC molecule.

The analysis of the [Al, H, C, N] PES gives that HAINC (<sup>2</sup>A') is the lowest lying isomer followed by HAICN (<sup>2</sup>A'), which is only 1.18 kcal mol<sup>-1</sup> higher in energy at the CCSD

(T)/aug-cc-pVTZ level, and therefore both isomers are the most relevant from an experimental point of view. For HAINC (<sup>2</sup>A') and HAICN (<sup>2</sup>A'), additional calculations at different coupled cluster levels of theory and through the composite procedure were performed to determine structural parameters and relative energies; these results are collected in Table 2. We can see a relatively good agreement among the geometrical parameters computed at the different levels. As expected, we can observe that the results obtained with the explicitly correlated couplet cluster theory (CCSD(T)-F12/cc-pVTZ-F12) are closer to those obtained at the CCSD(T)/aug-cc-pV(5+d)Z level than those obtained at the CCSD(T)/cc-pVTZ level without the F12 treatment. Adding tight d functions to the

**Table 3**

Energy of the Dissociation Processes for the Most Stable [Al, C, H, N] Isomers in eV Calculated at the CCSD(T)/aug-cc-pVTZ Level. ZPV Energies are Included at the Same Level

Processes	$\Delta E$
HAINC $\rightarrow$ AIH+CN	3.68
HAICN $\rightarrow$ AIH+CN	3.63
AINCH $\rightarrow$ AI+HCN	0.80
AICNH $\rightarrow$ AI+HNC	0.87
c-H-CAIN $\rightarrow$ AI+HCN	0.76
c-H-NAIC $\rightarrow$ AI+HNC	0.71
AIHCN $\rightarrow$ AI+HCN	0.10
AIHNC $\rightarrow$ AI+HNC	0.17

aluminum causes the distances where this atom is involved to vary slightly. The results obtained at the composite level show that the extrapolation of the basis set, the inclusion of CV correlation, and relativistic effects are important when calculating the geometries in these systems.

As in our previous studies on hydrides of zinc, iron, titanium, and calcium cyanide/isocyanide (Redondo et al. 2015, 2016, 2019, 2020), we can observe that the interaction between the aluminum atom of HAl and the CN unit to give HAICN slightly reinforces the C–N bond, whereas it is slightly weakened for HAINC where the bonding takes place through the nitrogen atom (the experimentally determined C–N bond distance in the cyano radical, CN, is 1.1718 Å; Huber & Herzberg 1979). The Al–H bond is reinforced in both isomers when the AIH molecule interacts with the CN one (the Al–H experimental bond distance for aluminum hydride, AIH, is 1.6478 Å; Huber & Herzberg 1979).

From the relative energies shown in Table 2, we also realize that hydroaluminum isocyanide, HAINC ( $^2A'$ ), is the lowest lying isomer at all the levels employed. If we focus on the effect of the different contributions on the relative energies, we can see that the addition of diffuse functions in the basis sets stabilizes the isocyanide isomer, HAINC, over cyanide, HAICN. When quadruple-zeta or higher bases are used, very similar values for the relative energy are obtained. On the other hand, the relative energy obtained at the CCSD(T)-F12/cc-pVTZ-F12 level (with a triple-zeta basis set) is almost equal to that calculated at the composite level. Thus, the energy difference between HAINC and HAICN goes from 1.09 kcal mol<sup>-1</sup> at the CCSD(T)/cc-pVTZ level to 1.40 kcal mol<sup>-1</sup> at the composite one.

### 3.2. Dissociation and Isomerization Processes

First, we analyze the stability of the [Al, C, H, N] isomers in terms of the adiabatic dissociation energies considering for each isomer the formation of the most stable products. The dissociation energies calculated at the CCSD(T)/aug-cc-pVTZ level are collected in Table 3. This table shows that all isomers are stable against fragmentation because all computed energies are positives. The dissociation energies of the HAICN/HAINC isomers to give HAl+CN are the highest, 3.68 and 3.63 eV (83.79 and 84.97 kcal mol<sup>-1</sup>), respectively; therefore, both isomers are the most stable against dissociation. The stability toward dissociation of the isomers originated from the interaction of the aluminum atom with HCN or HNC is similar. In both cases, the most stable isomer corresponds to the result of the linear interaction of the Al atom with the C or N

atom, AINCH/AICNH. The corresponding interaction through the C–N bond giving c-H-CAIN/c-H-NAIC is less stable. The AIHCN/AIHNC isomers are clearly the least stable upon dissociation, their dissociation energies being only 0.10 and 0.17 eV (2.22 and 3.87 kcal mol<sup>-1</sup>), respectively. These low values are consistent with the large Al–H bond distances obtained in these isomers (see Figure 1). These results of the stability in terms of the dissociation energies (Table 3) suggest that the most relevant isomers from an experimental point of view will be HAICN and HAINC.

We will now analyze the isomerization processes between the different isomers. The corresponding profiles, computed at the CCSD(T)/aug-cc-pVTZ level, are shown in Figure 2. The reaction profile corresponding to the interconversion of the two most stable isomers, hydroaluminum cyanide/isocyanide, HAICN/HAINC, is shown in panel (a). As can be seen, isomerization of HAICN to the more stable isomer HAINC involves transition state TS1, which is located 10.0 kcal mol<sup>-1</sup> ( $\sim$ 5032 K) above the HAICN isomer. Therefore, isomerization will not be a viable process under the conditions of the interstellar medium and, both isomers, if they are produced, could be present in the interstellar medium. We have also looked at isomerization processes involving the more stable isomers, HAICN and HAINC, and those resulting from the interaction of the Al atom with HCN or HNC. The isomerization processes between the isomer HAICN and those arising from the interaction of Al with HCN are shown in panel (b) whereas in panel (c) the analogous between the lowest-lying isomer, HAINC, and the isomers originating from the interaction of Al with HNC are reported. As can be seen in Figure 2 (panels (b) and (c)), the isomerization profile is similar for hydroaluminum cyanide and hydroaluminum isocyanide. All the interconversion processes between the isomers considered involve net activation barriers. The lowest barrier obtained corresponds to the c-H-CAIN  $\rightarrow$  AINCH process. The associated transition state, TS2-c, is located 2.8 kcal mol<sup>-1</sup> ( $\sim$ 1409 K) above the c-H-CAIN isomer. In view of the results shown in Figure 2, the isomerization processes considered will not be feasible at the temperature conditions of the interstellar medium. Therefore, obtaining HAICN or HAINC from isomerization of AIHCN or AIHNC are not viable processes. The formation of HAICN and HAINC isomers could take place by, analogous routes to those proposed for AINC (Petrie 1996) and, MgNC, MgCN, HMgNC, and MgC<sub>3</sub>N (Cernicharo et al. 2019b). That is, association of the metal ion (Al<sup>+</sup>) with cyanopolynes (NC<sub>2n+1</sub>H) and the subsequent dissociative recombination of the corresponding complex, with electrons.

### 3.3. Spectroscopic Parameters for Laboratory or Astronomical Detection

In this section, we will provide a high-level computed set of rotational spectroscopic parameters for the most stable HAICN and HAINC interstellar candidates to guide the spectral searches. We first calculated the equilibrium ( $A_e$ ,  $B_e$  and  $C_e$ ) and then the ground state ( $A_0$ ,  $B_0$  and  $C_0$ ) rotational constants were computed by adding the vibrational correction, which is estimated from the vibration–rotation coupling constants and degeneracy factors of the vibrational modes. The rotation–vibration coupling constants are computed from the full anharmonic cubic force field (CFF). The calculated values of the equilibrium and ground state rotational constants are shown in Table 4. The quasilinear disposition of the atoms inferred

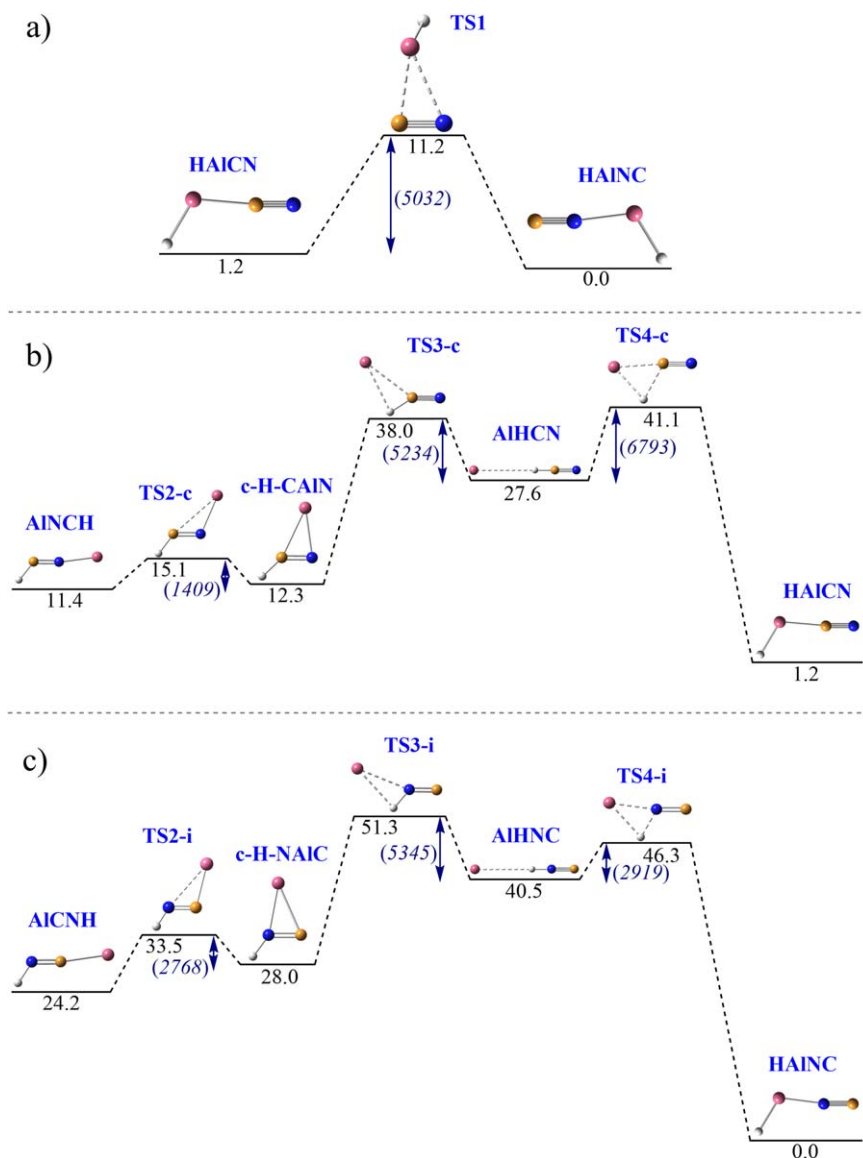


**Figure 2.** Energy profile for the isomerization process between [Al, C, H, N] isomers. Relative energies, in  $\text{kcal mol}^{-1}$ , are calculated with respect to HAINC at the CCSD(T)/aug-cc-pVTZ level. The isomerization barriers (in eV) are indicated by a double arrow in blue italic.

from the geometrical parameters of both HAICN and HAINC can also be seen in the values of the rotational constants, which will be translated in expected characteristic patterns of intense a-type R-branch  $(J+1)_{0,J+1} \leftarrow J_{0,J}$  transitions (spaced by roughly  $\sim B + C$ ). In addition, we collect in Table 4 the quartic centrifugal distortion parameters in the Watson's S-reduced Hamiltonian ( $D_J, D_{JK}, D_K, d_1$  and  $d_2$ ) as well as the  $^{14}\text{N}$  and  $^{27}\text{Al}$  nuclear quadrupole coupling constants ( $\chi$ ), the electron spin–nuclear spin (T), and the Fermi Contact ( $b_f$ ) parameters, which were computed at the CCSD/aug-cc-pVQZ level taking the composite geometry. It is worth noticing that similar levels of theory have been already established as suitable methods to correctly reproduce the molecular geometry of different metal bearing species (Cernicharo et al. 2019b). We also calculated the electron-spin-rotation ( $\varepsilon$ ) parameters and the nuclear-spin-rotation (C) constants, employing in this case a MP2 method (Møller & Plesset 1934), which is the highest level implemented in the GAUSSIAN 16 program package (Frisch et al. 2016). Taken together, this high-level theoretical information is mandatory to achieve an eventual laboratory

detection and may even enable to perform a first radio astronomical search using the spectral line survey as a conventional laboratory spectrum. In this context, and to guide spectral searches, we have simulated the rotational spectrum for both isomers up to 50 GHz from the computed parameters presented in Table 4 (shown in Figure 3) employing the SPCAT program (Pickett 1991).

At this stage, additional comments should be done regarding the fine and hyperfine structure to help in the analysis and assignment of the laboratory spectrum. The rotational levels of the  $^2A'$  states of hydroaluminum isocyanide are split into two fine structure components due to electronic-spin-rotation interactions. Moreover, these levels are subsequently split due to the nuclear quadrupole interaction of both the  $^{14}\text{N}$  and  $^{27}\text{Al}$  nuclei along with the corresponding electron spin–nuclear spin, nuclear-spin rotation and Fermi contact couplings, therefore resulting in a hyperfine structure of extraordinary complexity. Although, at very high frequencies part of the hyperfine patterns shall collapse giving rise to observable line clusters of considerably broad line widths. Apart from these fine and

**Table 4**

Spectroscopic Parameters for the Lowest Lying [Al, C, H, N] Isomers (in MHz): Equilibrium Rotational Constants ( $A_e$ ,  $B_e$  and  $C_e$ ) and Rotational Constants for the Ground Vibrational State ( $A_0$ ,  $B_0$  and  $C_0$ ) are Computed with the Composite Method

Parameters	HAINC	HAICN	Parameters	HAINC	HAICN
$A_e$	262050.0	265880.1	$b_f$ ( $^{14}\text{N}$ )	18.2	1.0
$B_e$	5887.7	5062.4	$b_f$ ( $^{27}\text{Al}$ )	896.5	860.4
$C_e$	5758.4	4967.8	$b_f$ ( $^1\text{H}$ )	220.7	173.8
$A_0$	264214.8	268645.5	$C_{aa}$ ( $^{14}\text{N}$ ) $\times 10^2$	0.20	0.90
$B_0$	5903.3	5066.5	$C_{bb}$ ( $^{14}\text{N}$ ) $\times 10^2$	0.11	0.12
$C_0$	5767.3	4966.6	$C_{cc}$ ( $^{14}\text{N}$ ) $\times 10^2$	0.10	0.12
$D_J \times 10^3$	2.18	1.86	$C_{ab} + C_{ba}$ ( $^{14}\text{N}$ ) $\times 10^2$	0.041	0.41
$D_{JK}$	1.20	0.21	$C_{ab} - C_{ba}$ ( $^{14}\text{N}$ ) $\times 10^2$	-0.030	-0.42
$D_K$	70.17	84.52	$C_{aa}$ ( $^{27}\text{Al}$ )	0.26	0.29
$d_1 \times 10^3$	-5.51	0.035	$C_{bb}$ ( $^{27}\text{Al}$ ) $\times 10^2$	0.29	0.30
$d_2 \times 10^4$	-10.36	-0.051	$C_{cc}$ ( $^{27}\text{Al}$ ) $\times 10^2$	0.33	0.30
$\varepsilon_{aa}$	2635.2	3146.9	$C_{ab} + C_{ba}$ ( $^{27}\text{Al}$ ) $\times 10^1$	-2.3	-2.5
$\varepsilon_{bb}$	7.8	9.4	$C_{ab} - C_{ba}$ ( $^{27}\text{Al}$ ) $\times 10^1$	2.2	2.5
$\varepsilon_{bb}$	8.6	1.6	$C_{aa}$ ( $^1\text{H}$ ) $\times 10^2$	-0.84	-0.77
$\varepsilon_{ab} + \varepsilon_{ba}$	-980.3	-1127.5	$C_{cc}$ ( $^1\text{H}$ ) $\times 10^3$	-0.40	-0.36
$\varepsilon_{ab} - \varepsilon_{ba}$	945.6	1079.8	$C_{ab} + C_{ba}$ ( $^1\text{H}$ ) $\times 10^2$	-1.5	-1.6
$\chi_{aa}$ ( $^{14}\text{N}$ )	-1.9	-5.6	$C_{ab} - C_{ba}$ ( $^1\text{H}$ ) $\times 10^2$	1.4	1.6
$\chi_{bb} - \chi_{cc}$ ( $^{14}\text{N}$ )	-0.090	-0.73	$\mu_a$	3.3	3.7
$\chi_{ab}$ ( $^{14}\text{N}$ )	0.28	0.064	$\mu_b$	0.5	0.5
$\chi_{aa}$ ( $^{27}\text{Al}$ )	-18.6	-19.6	$\mu_c$	0.0	0.0
$\chi_{bb} - \chi_{cc}$ ( $^{27}\text{Al}$ )	-53.4	-56.4			
$\chi_{ab}$ ( $^{27}\text{Al}$ )	68.4	7.6			
$T_{aa}$ ( $^{14}\text{N}$ )	2.5	0.21			
$T_{bb} - T_{cc}$ ( $^{14}\text{N}$ )	-1.0	5.0			
$T_{ab}$ ( $^{14}\text{N}$ )	1.3	-2.1			
$T_{aa}$ ( $^{27}\text{Al}$ )	-28.7	-26.3			
$T_{bb} - T_{cc}$ ( $^{27}\text{Al}$ )	124.6	128.4			
$T_{ab}$ ( $^{27}\text{Al}$ )	50.6	56.0			
$T_{aa}$ ( $^1\text{H}$ )	0.068	0.65			
$T_{bb} - T_{cc}$ ( $^1\text{H}$ )	8.2	8.7			
$T_{ab}$ ( $^1\text{H}$ )	-2.4	-2.1			

**Note.** Centrifugal distortion parameters in the  $S$ -reduced Hamiltonian ( $D_J$ ,  $D_{JK}$ ,  $D_K$ ,  $d_1$ , and  $d_2$ ). The elements of the  $^{14}\text{N}$  and  $^{27}\text{Al}$  nuclear quadrupole coupling tensor ( $\chi$ ), the elements of the electron spin—nuclear spin tensor ( $T$ ), the Fermi contact couplings ( $b_f$ ), and the dipole moment components ( $\mu$  in Debye) are computed at the CCSD/aug-cc-pVQZ level, while the elements of the electron spin—molecular rotation tensor ( $\varepsilon$ ) and the nuclear-spin-rotation ( $C$ ) constants are computed using the MP2/aug-cc-pVQZ level at the composite geometry. We have provided a full list of the relevant spectroscopic parameters to rotational spectroscopy. Nevertheless, some of them (i.e., the diagonal elements of the  $^{14}\text{N}$  nuclear quadrupole coupling tensor) are usually not attainable from the experimental data.

hyperfine couplings, a Zeeman effect might be expected to affect both HAINC and HAICN systems. Thus, in order to carry out eventual experimental measurements of these molecules, and besides an experimental study by means of infrared spectroscopy, we suggest as a potential alternative to perform a Fourier-transform microwave experiment. This approach has been previously employed to study the rotational spectra of related molecular systems such as AlNC, AlC<sub>3</sub>N (Ziurys et al. 2002; Cabezas et al. 2014) as well as other metal derivatives, i.e., ZnCN and HZnCN (Sun et al. 2009). A future laboratory characterization will allow to perform a more confident interstellar search for the target species at centimeter wavelengths, employing the Yebes 40 m or GBT 100 m radio telescopes, using, for instance, some the latest line spectral survey of IRC+10216 (Pardo et al. 2021b), which presents several unidentified lines (U-lines) at the  $5\sigma$  level and around 50 features at the  $3\sigma$  level. Regarding an estimation of the accuracy of the spectral predictions, the lack of available experimental information of the systems under study does not enable us to provide a true assessment of the accuracy estimation for the rest frequencies. Several studies have been reported related to this topic, highlighting the study of  $S$ -bearing species (Alessandrini et al. 2018) where the authors

employ different composite schemes and analyze systematic errors related to the rotational constant values. For instance, they point out that for CCS, errors of about 4 MHz are predicted for very low frequencies, while deviations of  $\sim 100$  MHz are observed for frequencies above the submillimeter-wave region (300 GHz), showing deviation of approximately 0.04% for species such as C<sub>3</sub>S, C<sub>4</sub>S, and C<sub>5</sub>S. Furthermore, we can employ the spectroscopic data benchmarked by Redondo et al. (2015) for the related hydrozinc cyanide isomer HZnCN. A scaling factor of 0.9900 bring the experimental value of the rotational constant in agreement with the CCSD(T)/CBS predicted one. Thus, if we assume that the uncertainties in the rest frequencies are approximately transferable to our systems, we can estimate the upper limit errors of  $\sim 70$  MHz for very low frequencies (centimeter-wave region). However, despite the uncertainty in the absolute frequency scale, the predicted hyperfine structure of the rotational spectrum of HAINC and HAICN can be used as a key pattern to identify these species in laboratory (terrestrial) experiments as well as, eventually, in the ISM.

Finally, in a quest to guide an eventual characterization of the lowest lying [Al, H, C, N] isomers using infrared (IR) spectroscopy, we provide the harmonic ( $\omega$ ) and anharmonic ( $\nu$ )

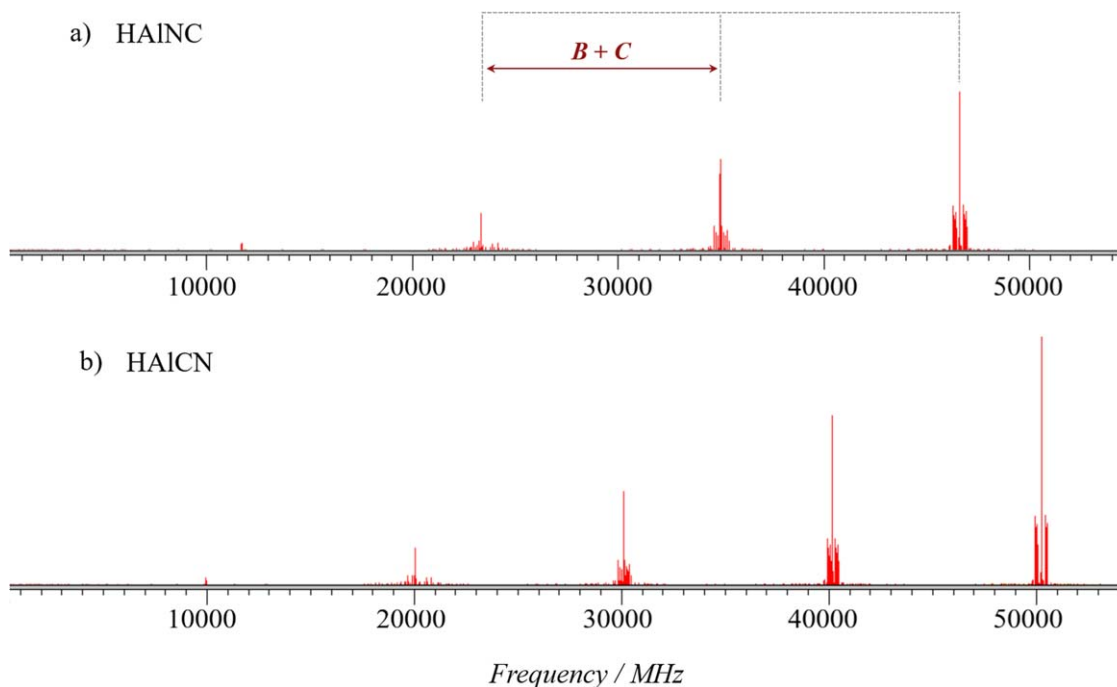


**Figure 3.** Predicted synthetic rotational spectrum of HAINC [inset (a)] and HAICN [inset (b)] at 10 K in the 0–50 GHz frequency range, computed based on the theoretically determined spectroscopic parameters listed in Table 4.

**Table 5**

Harmonic,  $\omega$ , and Anharmonic,  $\nu$ , Vibrational Frequencies ( $\text{cm}^{-1}$ ) and IR Intensities ( $\text{km mol}^{-1}$ ), for the Lowest Lying [Al, C, H, N] Isomers Calculated at the CCSD (T)/aug-cc-pVTZ Level

Mode	HAINC				Mode	HAICN <sup>a</sup>			
	$\omega$	$I_{\text{har}}$	$\nu$	$I_{\text{anhar}}$		$\omega$	$I_{\text{har}}$	$\nu$	$I_{\text{anhar}}$
a'' out-of-plane bending	130	1.8	125	1.5	a'' out-of-plane bending	193	4.0	201	3.8
a' AINC bending	154	1.8	147	1.5	a' AICN bending	214	5.0	220	5.1
a' HAIN bending	580	45.1	573	51.6	a' AIC stretching	522	50.6	527	39.9
a' AIN stretching	618	209.2	611	198.7	a' HAIC bending	598	157.5	589	159.2
a' HAI stretching	1869	155.5	1792	148.1	a' AIH stretching	1891	152.5	1897	152.6
a' CN stretching	2077	309.2	2048	299.0	a' CN stretching	2252	30.2	2224	28.9

**Note.**

<sup>a</sup> Anharmonic contributions for HAICN are calculated at the B2PLYP/aug-cc-pVTZ level.

vibrational frequencies along with the corresponding IR intensities, shown in Table 5. We calculated the harmonic vibrational frequencies and the anharmonic contributions at the CCSD(T)/aug-cc-pVTZ level. Anharmonic contributions are often required to model a trustworthy IR spectrum.

HAINC and HAICN shows different vibrational patterns, and both isomers have several high-intensity modes suggesting their detection in space through IR spectroscopy could be likely. In the lowest energy isomer, HAINC, the most intense band corresponds to the CN stretching mode ( $\nu = 2048 \text{ cm}^{-1}$ ), and the AIN stretching mode ( $\nu = 611 \text{ cm}^{-1}$ ) also presents a high intensity. In HAICN, the HAIC bending mode ( $\nu = 589 \text{ cm}^{-1}$ ) is the most intense in IR, and the HAI stretching mode ( $\nu = 1897 \text{ cm}^{-1}$ ) also gives rise to a strong IR absorption band. As was also found in similar systems (Redondo et al. 2015), the IR intensities of the frequencies associated to the C–N stretching mode for HAINC and HAICN are clearly different, with the IR band for HAINC being much stronger ( $I_{\text{anhar}} = 299.0 \text{ km mol}^{-1}$ ) than that for the HAICN molecule ( $I_{\text{anhar}} = 28.9 \text{ km mol}^{-1}$ ). These discrepancies arise from the different nature of the CN bond in HAINC and HAICN and are

related to the C–N bond distances. As it can be seen from Table 2, the C–N bond distance in the isomer with an isocyanide arrangement, HAINC (1.1785 Å at the composite level) is slightly larger than that in the cyano radical, CN, in which the experimental bond distance is 1.1718 Å (Huber & Herzberg 1979). The opposite occurs for the corresponding isomer with a cyanide arrangement, HAICN (the C–N bond distance is 1.1620 Å at the composite level). Regarding anharmonicity, we observe that, for HAINC, the harmonic frequencies are slightly higher than the corresponding anharmonic ones and the absolute differences are more important in the stretching frequencies than in the bending ones. Whereas negative anharmonicities were found in mostly vibration modes of the HAICN isomer.

#### 4. Conclusions

We have carried out a theoretical study of the doublet and quartet PESs of the [Al, H, C, N] system using accurate quantum chemistry approaches. We have studied 11 different structures, ranging for linear or bent structures with the

aluminum atom located at one end of the molecule or in a middle position, to cyclic (three-member ring) structures. We have obtained that doublet electronic states are more stable than the quartet ones, with the only exception of the isomers HCAIN and HNAIC where the quartet state is slightly more stable than the doublet one. These isomers are the least stable and are no relevant from an experimental point of view.

All levels of theory predict hydroaluminum isocyanide in its doublet state, HAINC ( $^2A'$ ), to be the lowest-lying isomer followed by hydroaluminum cyanide, HAICN ( $^2A'$ ), which is only  $1.59 \text{ kcal mol}^{-1}$  ( $0.0689 \text{ eV}$ ) above, at the composite level. These isomers can be seen as the result of the linear interaction between the aluminum atom of hydroaluminum, HAl, and the cyano radical through either the carbon atom or the nitrogen atom.

The six isomers that arise from the interaction either linear or through the C–N bond between the aluminum atom and hydrogen cyanide/isocyanide HCN/HNC are located above hydroaluminum cyanide/isocyanide, HAICN/HAINC, (over  $11 \text{ kcal mol}^{-1}$ ). For these isomers, the linear interaction of aluminum with N/C is slightly more stable than that occurring through the C–N bond, and the least stable isomers are obtained from the linear interaction of Al with the terminal H atom. In general, we observe that the isomers resulting from the interaction of aluminum with HCN are more stable (about  $14 \text{ kcal mol}^{-1}$ ) than those obtained from HNC.

The results of the isomers stability in terms of the dissociation energies show that the highest values correspond to the dissociation of the HAICN/HAINC isomers to give HAl + CN ( $3.68$  and  $3.63 \text{ eV}$  at the CCSD(T)/aug-cc-pVTZ level, respectively). The isomerization process between HAICN and HAINC involves transition state TS1 (located  $10.0 \text{ kcal mol}^{-1}$  ( $5032 \text{ K}$ ) above HAICN at the CCSD(T)/aug-cc-pVTZ level) and will not be a viable process under the conditions of the interstellar medium. Therefore, both HAINC and HAICN isomers are the most relevant from an experimental point of view. For these isomers, we provide accurate predictions for their molecular structure and vibrational and rotational spectroscopic parameters that could aid in their experimental identification in the laboratory or in space.

Herein, we have provided a complete set of the relevant spectroscopic parameters to rotational spectroscopy for the lowest in energy isomers HAINC and HAICN, highlighting the calculation of theoretical rotational constants with the so-called “spectroscopic” accuracy at the composite level. Moreover, we have computed all the fine and hyperfine parameters to guide eventual spectral (laboratory or space-based) searches for these Al-bearing species, which are needed to interpret their incredibly complex hyperfine structure. Within this framework, we are now able to perform a first radio astronomical search for both isomers using the newly determined theoretical spectroscopic constants and employing some of the latest line surveys with unprecedented sensitivities, such as the ultra-deep spectral survey of IRC+10216 (Pardo et al. 2021b), as a “laboratory” spectrum. Finally, we present the vibrational frequencies along with the corresponding IR intensities computed at the CCSD(T) level and taking into account anharmonic corrections. We hope these results will benefit the astrophysical community by allowing the laboratory or interstellar detection of these appealing interstellar candidates.

Financial support from the Spanish Ministerio de Ciencia e Innovación (PID2020-117742GB-I00) and Junta de Castilla y Leon (grant VA244P20) is gratefully acknowledged. M.S.N acknowledges funding from the Spanish Ministerio de Ciencia, Innovación y Universidades under predoctoral FPU grant (FPU17/02987)

## ORCID iDs

Pilar Redondo  <https://orcid.org/0000-0001-7876-4818>  
 Miguel Sanz-Novo  <https://orcid.org/0000-0001-9629-0257>  
 Carmen Barrientos  <https://orcid.org/0000-0003-0078-7379>

## References

- Alessandrini, S., Gauss, J., & Puzzarini, C. 2018, *J. Chem. Theory Comput.*, **14**, 5360
- Becke, A. D. 1988, *JChPh*, **88**, 2547
- Cabezas, C., Barrientos, C., Largo, A., et al. 2014, *JChPh*, **141**, 104305
- Cabezas, C., Cernicharo, J., Alonso, J. L., et al. 2013, *ApJ*, **775**, 133
- Cernicharo, J., Angúdez, M., Kaiser, R. I., et al. 2021a, *A&A*, **652**, L9
- Cernicharo, J., Cabezas, C., Endo, Y., et al. 2021b, *A&A*, **650**, L14
- Cernicharo, J., Cabezas, C., Pardo, J. R., et al. 2019b, *A&A*, **630**, L2
- Cernicharo, J., & Julín, M. 1987, *A&A*, **183**, L10
- Cernicharo, J., Velilla-Prieto, L., Agúdez, M., et al. 2019a, *A&A*, **627**, L4
- Douglas, M., & Kroll, N. 1974, *AnPhy*, **82**, 89
- Dunning, T. H. 1989, *JChPh*, **90**, 1007
- Dunning, T. H., Peterson, K. A., & Wilson, A. K. 2001, *JChPh*, **114**, 9244
- Fortenberry, R. C., Trabelsi, T., & Francisco, J. S. 2020, *JPCA*, **124**, 8834
- Frisch, M. J., Trucks, G. W., Schlegel, H. B., et al. 2016, Gaussian 16, Revision B+01 (Wallingford, CT, USA: Gaussian)
- Grimme, S., Ehrlich, S., & Goerigk, L. 2011, *JCoCh*, **32**, 1456
- Grimme, S. J. 2006, *ChPh*, **124**, 034108
- Guélin, M., Cernicharo, J., Kahane, C., & Gomez-Gonzalez, J. 1986, *A&A*, **157**, L17
- Guélin, M., Lucas, R., & Cernicharo, J. 1993, *A&A*, **280**, L19
- Guélin, M., Muller, S., Cernicharo, J., et al. 2000, *A&A*, **363**, L9
- Guélin, M., Muller, S., Cernicharo, J., et al. 2004, *A&A*, **426**, L49
- Hehre, W. J., Radom, L., Schleyer, P. V. P., & Pople, J. A. 1986, *Ab Initio Molecular Orbital Theory* (New York: Wiley) pp 65
- Helgaker, T., Klopper, W., Koch, H., & Noga, J. 1997, *JChPh*, **106**, 9639
- Huber, K. P., & Herzberg, G. 1979, *Molecular Spectra and Molecular Structure. IV. Constants of Diatomic Molecules* (New York: Van Nostrand Reinhold Co.)
- Jiang, W., DeYonker, N. J., & Wilson, A. K. 2012, *JCTC*, **8**, 460
- Kawaguchi, K., Kagi, E., Hirano, T., et al. 1993, *ApJL*, **406**, L39
- Knizia, G., Adler, T. B., & Werner, H.-J. 2009, *JChPh*, **130**, 054104
- Lee, C., Yang, W., & Parr, R. G. 1988, *PhRvB*, **37**, 785
- Lee, K. L. L., Changala, P. B., Loomis, R. A., et al. 2021, *ApJ*, **910**, L2
- Lee, T. J., & Taylor, P. R. 1989, *Int. J. Quant. Chem. Symp.*, **36**, 199
- Loomis, R. A., Burkhardt, A. M., Shingledecker, C. N., et al. 2021, *NatAs*, **5**, 188
- Mauron, N., & Huggins, P. J. 2010, *A&A*, **513**, A31
- McGuire, B. A. 2018, *ApJS*, **239**, 2
- Mills, I. M. 1972, in *Vibration-Rotation Structure in Asymmetric and Symmetric-Top Molecules. In Molecular Spectroscopy: Modern Research*, ed. K. N. Rao & C. W. Mathews (New York: Academic Press), 115
- Møller, C., & Plesset, M. S. 1934, *PhRv*, **46**, 618
- Pardo, J. R., Cabezas, C., Fonfría, J. P., et al. 2021a, *A&A*, **652**, L13
- Pardo, J. R., Cernicharo, J., Tercero, B., et al. 2021b, *A&A*, **658**, A39
- Peng, H., & Hirao, K. 2009, *JChPh*, **130**, 044102
- Peterson, K. A., Adler, T. B., & Werner, H. J. 2008, *JChPh*, **128**, 084102
- Petrie, S. 1996, *MNRAS*, **282**, 807
- Pickett, H. M. 1991, *JMoSp*, **148**, 371
- Pulliam, R. L., Savage, C., Agúdez, M., et al. 2010, *ApJL*, **725**, L181
- Raghavachari, K., Trucks, G. W., Pople, J. A., & Head-Gordon, M. 1989, *CPL*, **157**, 479
- Redondo, P., Barrientos, C., & Largo, A. 2016, *ApJ*, **828**, 45
- Redondo, P., Barrientos, C., & Largo, A. 2019, *ApJ*, **871**, 180
- Redondo, P., Largo, A., & Barrientos, C. 2020, *ApJ*, **899**, 135
- Redondo, P., Largo, A., Vega-Vega, A., & Barrientos, C. 2015, *JChPh*, **142**, 184301
- Sanz, M. E., McCarthy, M. C., & Thaddeus, P. 2002, *ApJL*, **577**, L71

- Stanton, J. F., Gauss, J., Harding, M. E., & Szalay, P. G. 2013, CFOUR, A Quantum Chemical Program Package <http://www.cfour.de/>
- Sun, M., Apponi, A. J., & Ziurys, L. M. 2009, *JChPh*, **130**, 034309
- Tenenbaum, E. D., & Ziurys, L. M. 2009, *ApJL*, **694**, L59
- Tenenbaum, E. D., & Ziurys, L. M. 2010, *ApJL*, **712**, L93
- Trabelsi, T., Davis, M. C., Fortenberry, R. C., & Francisco, J. S. 2019, *JChPh*, **151**, 244303
- Tsuji, T. 1973, *A&A*, **23**, 411
- Turner, B. E. 1991, *ApJ*, **376**, 573
- Watrous, A. G., Davis, M. C., & Fortenberry, R. C. 2021, *FrASS*, **8**, 643348
- Watson, J. K. 1968, *MPh*, **15**, 479
- Werner, H.-J., & Knowles, P. J. 1985a, *JChPh*, **82**, 5053
- Werner, H.-J., & Knowles, P. J. 1985b, *CPL*, **115**, 259
- Werner, H.-J., Knowles, P. J., Knizia, G., et al. 2015, MOLPRO, v2015.1, a package of ab initio programs <https://www.molpro.net/>
- Werner, H.-J., Knowles, P. J., Knizia, G., Manby, F. R., & Schütz, M. 2012, *WIREs Comput. Mol. Sci.*, **2**, 242
- Woon, D. E., & Dunning, T. H. 1993, *JChPh*, **98**, 1358
- Zack, L. N., Halfen, D. T., & Ziurys, L. M. 2011, *ApJL*, **733**, L36
- Ziurys, L. M., Apponi, A. J., Guélin, M., & Cernicharo, J. 1995, *ApJL*, **445**, L47
- Ziurys, L. M., Savage, C., Highberger, J. L., et al. 2002, *ApJL*, **564**, L45